# Bio-based honeycomb panel with core in Arundo donax rings and flax/epoxy composite skins: mechanical tests and numerical analysis

L Crociati<sup>1</sup>, G Donini<sup>1\*</sup>, T Jeannin<sup>2</sup>, V Placet<sup>2</sup>, L Molari<sup>1</sup>

- <sup>1</sup> DICAM Univeristy of Bologna. Viale del Risorgimento 2, Bologna, Italy.
- <sup>2</sup> Université de Franche-Comté, CNRS, institut FEMTO-ST, 25000, Besançon, France.
- \* Corresponding author's e-mail: giovanni.donini2@unibo.it

#### Abstract.

Honeycomb sandwich panels find widespread use in various applications of the building sector like non-structural lightweighted panels for partitions, floating floors, insulation panels or furniture. These panels typically consist of three layers: two thin, rigid external layers and a thick, low-density internal layer with a honeycomb geometric shape. To reduce environmental footprint, eco-friendly materials are encouraged. In this study, we propose a sandwich panel with a core made of Arundo donax rings and skins made of flax fibre reinforced epoxy composite. Arundo donax is an infesting very common reed in southern Europe environmentally advantageous due to its rapid growth, which gather a better CO<sub>2</sub> absorption then sequestrated in the panel. The honeycomb panels are produced by thermocompression and tested mechanically using pull-off tests and three-point bending. The influence of the surface roughness of the rings on the mechanical bending properties is investigated, focusing on the adhesion between skin and core, as well as between the individual Arundo donax rings within the core. The results show that polishing treatment significantly impacts all the flexural mechanical properties, especially when performed on lateral surfaces of the rings. In particular, the polishing treatment has increased the flexural strength of 24.25% shifting from 19.06 MPa to 25.16 MPa. Numerical simulations employing FEM with cohesive surface contacts between skins and Arundo donax rings are conducted to investigate the quasi static bending mechanical behaviour and the failure point of the sandwich panels. The model accurately replicates the experimental results while maintaining simplicity.

Keywords: Arundo donax, Flax fibre, Composite, Epoxy resin, Honeycomb panel, Abaqus, FEM, Sandwich panel.

## 1. Introduction

Honeycomb sandwich structures exhibit lightweight characteristics, high stiffness to weight and strength to weight ratios, effective thermal insulation, and strong load-bearing capabilities [1]. They find extensive applications in civil engineering, mechanical engineering, and aerospace due to their versatility [2]. Honeycomb panels represent a distinct type of sandwich panel, comprising three layers: two thin and highly rigid external layers, and a thick internal layer characterized by a honeycomb geometric shape, from which the panel derives its name. The physical and mechanical properties of honeycomb panels can exhibit considerable variability, stemming not only from the broad range of materials usable for the core and skins but also from geometric variations controllable during panel fabrication. These variations include thicknesses, the geometric shape of the core cells, and the connection they establish with the skins [3].

To reduce environmental footprint in structures, eco-friendly materials are encouraged. Some examples of eco-friendly applications in honeycomb boards can be found in the literature. Gato et al. 2021 [4] investigate the use of discarded bottle caps as core with hybrid glass fibre composite skins. The use of bottle caps exemplifies circularity through material reuse. A similar application, where bottle caps are used in the core but with flax-based laminates for the skins, is also examined by Oliveira et al. 2021[5]. Antony et al. 2020 [6] combine bio-based materials, hemp and polylactic acid (PLA), to manufacture a hemp/PLA 3D printed honeycomb sandwich structure. Napolitano et al. 2023 [7] show an example of partially bio-based sandwich panels made with bamboo core and synthetic skin made with aluminium. Fully bio-based sandwich panels are studied by Darzi, et al. 2020 [8] for boards made with plywood faces and bamboo core, using different schemes with one or two bamboo layers for the core, and by Fu et al. 2023 [9] which uses flax FRP for skins and paper honeycomb for the core.

In the present study, bio-based sandwich honeycomb panels with a core made of Arundo donax (hereinafter referred to as AD) rings glued with foaming epoxy resin to skins made of flax fibre reinforced epoxy composites are investigated, inspired by the idea proposed in [10] in which the core was made of bamboo rings.

In this perspective, the use of natural materials like bamboo or AD can be a viable alternative [11,12] to conventional construction materials like steel, concrete and wood. AD is a perennial herbaceous plant with a long, hollow, and robust stem that grows in even relatively poor soils. It belongs to the group of giant reeds, specifically within the family of Poaceae. Due to its high tolerance to different climates and environmental conditions, it can be found worldwide, mainly in southern Europe [11,13], that grows spontaneously, differently from bamboo species, which grows only if cultivated and are native from Asian and Latin America territories. Due to that, AD is involved in lower economic and environmental impacts, compared to bamboo. Additionally harvesting AD is simpler and can be done with threshers due to its size. The stem, called culm, is a hollow cylinder with diameters ranging from 1 to 3 cm, while the thickness of the walls varies between 1 and 4.5 mm, the culm is divided by diaphragms (named nodes) into internodes 12-30 cm long [14]. Inside the culm wall, sclerenchymatous fibres strengthen vascular bundles and are embedded in a matrix of lignified parenchyma [15] giving a good mechanical performance. Molari et al. [11] provided a mechanical characterization of AD. AD has a high growth rate, a good strength/weight ratio, excellent flexibility, and lightness characteristics compatible with the engineering requirements for use in civil construction. Regarding sustainability, by analyzing the life cycle of AD compared to pure wood, comes up that the growing time and the land use are lower, as well as the demand for water for production. The use of these raw materials is limited by their shapes and dimensions. Their use in laminated structures or panels can overcome this issue. In the field of panel engineering, García-Ortuno et al. [15] demonstrated the feasibility of producing particleboard in the engineering field using shredded AD particles as aggregates and urea formaldehyde resin as an adhesive, Cintura et al. [16] conducted a study on the physical and mechanical characteristics of chipboard panels made with chips of sodium silicate as resin [16]. In addition, the circular geometry of the Arundo donax stem could be exploited to develop a core for honeycomb sandwich structures.

For the skins natural fibers have many advantages over their synthetic counterparts, such as: sustainability [17], biodegradability, renewability [18], low cost [19], low density and specific mechanical properties suitable for secondary structural applications, poor electrical conductivity, good thermal and acoustic insulation. One of the most widely used plant fibre is flax, owing to its high mechanical properties and versatility. Flax (*Linum Usitatissimum*) has been widely utilized since prehistoric times [20][21]. Recently, it has been applied to prepreg textiles for technical applications, such as transport, wind energy, sports, and leisure. The flax fibers present an average length ranging from 20 to 30 mm, have a polygonal section with an average diameter of approximately 15µm [22]. The purpose of this study is to enhance the use of non-conventional bio-based locally native materials for the construction sector. The key properties of the panel are its lightness gathered by the honeycomb technology, its low environmental impact ensured by the use of bio-based materials like flax and AD and its good mechanical performance, provided by the use of AD rings and foaming epoxy resin, improving the adhesion between them by previously polishing the AD lateral surfaces.

The investigation of the proposed honeycomb sandwich focuses on the influence of the surface roughness of the rings on all the bending mechanical properties of the panels, considering the adhesion between skin and core, as well as between the different Arundo rings within the core. The pull-off method is used to assess the adhesion between the AD ring and flax/epoxy composite skin, while three-point bending tests serve to characterize the mechanical behaviour of the sandwich.

A Finite Element Model (FEM) is developed to better understand the nonlinear behavior of the panel and validated by comparing the load-displacement curves between experimental and numerical data. The aim is to develop a relatively simple FE model that can accurately represent the behavior of the panel up to the failure point, which can then be used in subsequent research for a parametric study concerning the core of the panel.

#### 2. Materials

## 2.1. Skins and core preparations

The skins (see Figure 1(a)) of sandwich panels are made of a combination of unidirectional flax fibre reinforcement with an areal weight of 110 g.m<sup>-2</sup> (FlaxTape<sup>TM</sup> from EcoTechnilin, France) and epoxy resin. The matrix is composed of the epoxy polymer SR Green Poxy 56, and the hardener SD 7561, provided by Sicomin (France), with a mass proportion of 100/36 in g. Composite plates are produced using hand lay-up and impregnation and a thermocompression process. For each plate, 3 FlaxTape plies are laid up forming unidirectional laminates. The plies are impregnated with an excess of the matrix in a steel mould measuring 300 × 200 mm<sup>2</sup>. Before this, the metallic parts are coated with Teflon to prevent resin adhesion to the mould. The FlaxTape plies are impregnated according to a specific protocol outlined in [23], aimed at optimizing impregnation while minimizing fibre waviness and misalignment. A resin strip is poured at the center of each ply perpendicular to the fibre direction. Under pressure, the matrix flows along the length of the fibres. The mould is then partially closed among two of its four lateral sides to allow excess matrix and trapped air to escape during the pressurization process. Subsequently, the mould is positioned between the platens of an AGILA® Presse 100 kN thermocompression press for curing. Once the mould reaches a temperature of 40 °C, a pressure of 3 bar is applied. After maintaining this temperature for 15 min, the mould is heated to reach the curing temperature of 100°C, which is held for 1 h. Heating is then discontinued, and the composite plate is allowed to cool naturally. Pressure is released at this temperature. Subsequently, a post-curing process is conducted in an oven at 100°C. Both skins of the same panel are manufactured simultaneously in the mould, separated by an intermediate iron sheet coated with Teflon.

The core (Figure 1(b)) is made of internode portions of AD,13 mm long. Each ring is cut with a circular saw and polished with different sandpapers. The polishing of the lateral surface (LS in the notation of the specimens) is done manually before cutting the cane (Figure 2). Two different sandpapers were used: Z80 and P120.

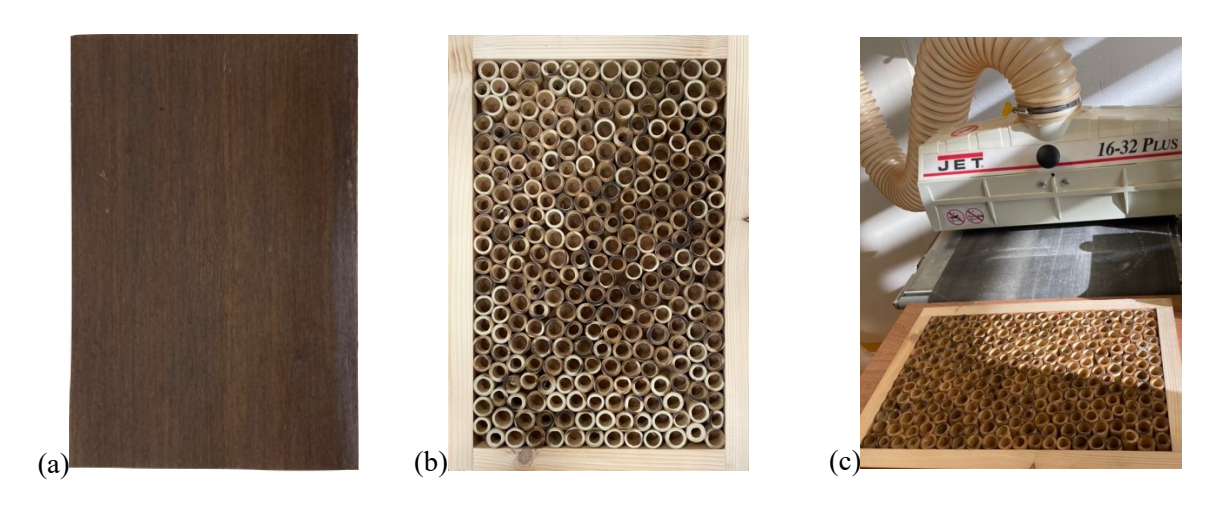


Figure 1. (a) Flax/epoxy composite skin; (b) AD rings for core in a frame (300mm x200mm) before polishing; (c) Polishing setup.

Considering 72 randomly taken rings of the core (highlighted in orange) in Figure 2, the outer diameters of the ring ranged from 13 mm to 17.1 mm (mean 15.2 mm), the inner diameters of the core from 8.2 mm to 12.6 mm (mean 10.7 mm), with a thickness from 1.45 mm to 3.5 mm (mean 1.5 mm).

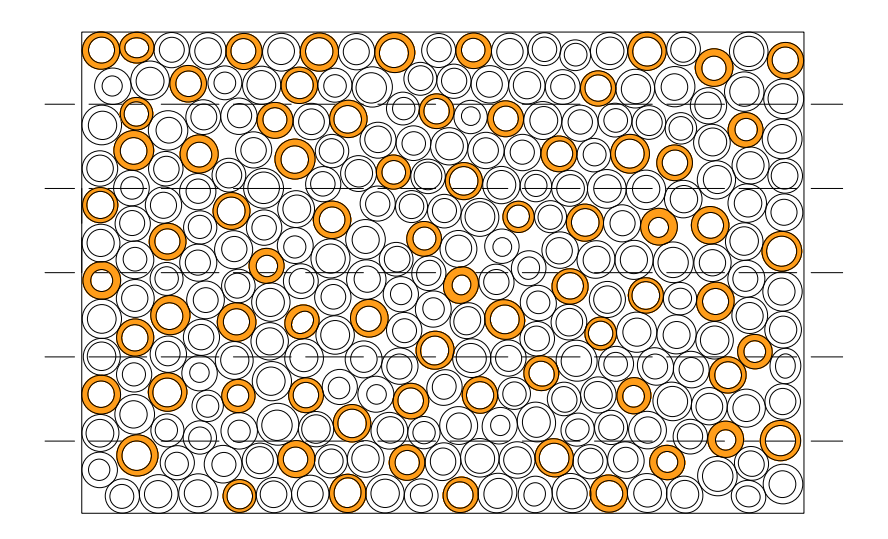


Figure 2. Core rings distribution and dimensions. Inner and outer diameter was measured for orange rings.

The sandwich is then obtained interposing the skin and the ring core as reported in Fig. 3

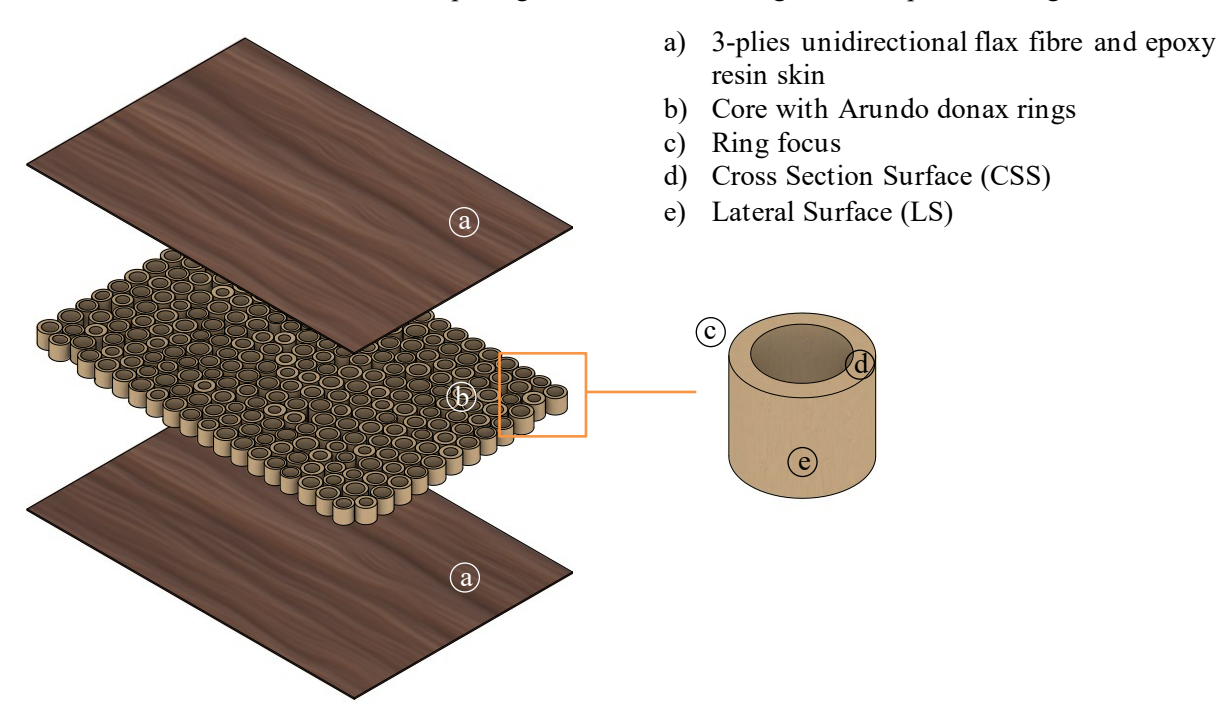


Figure 3. Detail of panel's components.

# 2.2. Sandwich panel preparation

To build the panels, all the rings constituting the core are posed in a wood frame of the same dimensions as the mould and the skins (300mm x 200mm) (Fig. 1(b)) and polished (Fig.1(c)) using a sanding and calibrating machine (JET 16-32 Plus) with P120 sandpaper.

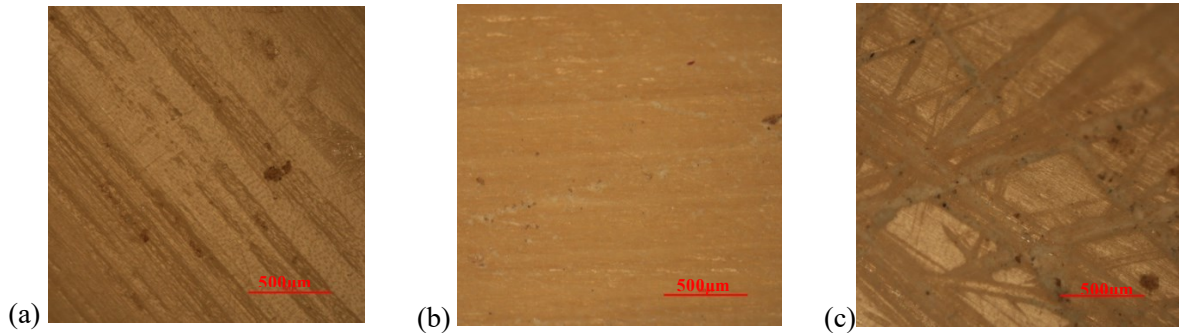


Figure 4. (a) Non-polished lateral surface; (b) P120 polished lateral surface; (c) Z80 polished lateral surface.

The sandwich panels (Fig. 5(b) and (c)) are then completed by two skins glued to the AD rings core with a foaming adhesive composed of 59.1 g of PB 170 glue and 18.8 g of DM02 hardener for one sandwich panel of 300 mm x 200 mm. The gluing process is applied by maintaining the panel at 100°C for 1 hour, using a pressure of 3 bar on the panel (Fig 5(a)). The glue becomes a foam that goes into the AD rings.

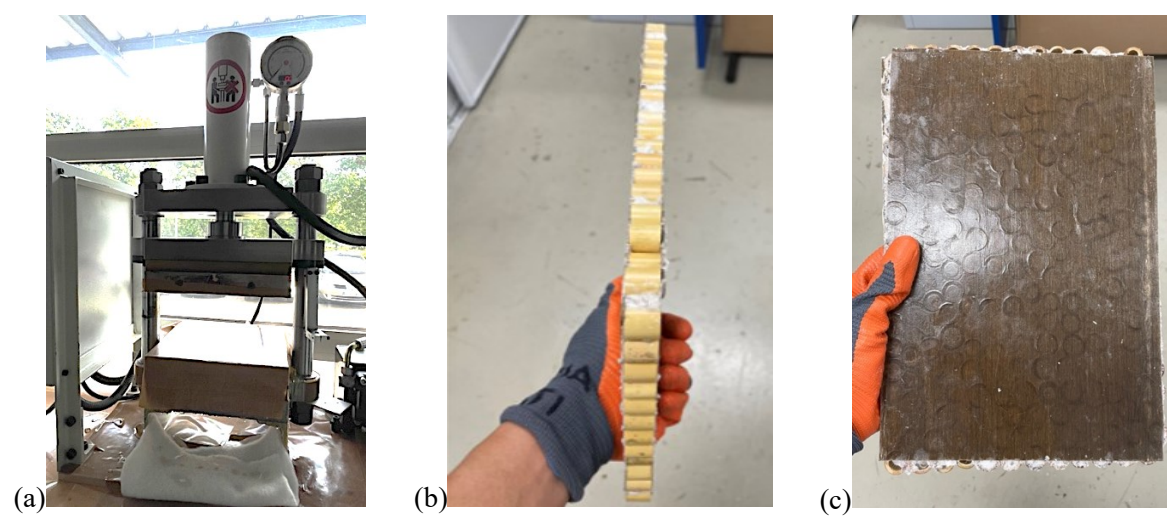


Figure 5 (a) Thermohydraulic press; (b) Sandwich panel core focus; (c) Sandwich panel skin focus.

Three types of panels were manufactured with a different treatment of the lateral surface of the core rings: the "Non-polished\_LS" with the lateral surfaces that did not receive any polishing (Fig. 4(a)), the "P120\_LS" and the "Z80\_LS" were treated respectively with P120 sandpaper and Z80 sandpaper in the ring's lateral surfaces (Fig. 3(b) and (c)). The Cross Section Surfaces (CSS) of all the rings in all the three panels received the same polishing with P120 sandpaper.

In particular, four samples with lateral surfaces non-polished, four samples with lateral surfaces polished with P120 sandpaper, and four samples with lateral surfaces polished with Z80 sandpaper were tested. The mean weights of the panels are reported in Table 1.

Rings lateral surface	Veight of sandwich panels		
polishing treatment	Core [g]	Skins x2 [g]	Total glue [g]
Non-polished_LS	190.7	82.5	70.9
Z80_LS	200.0	76.3	70.9
P120_LS	197.2	78.3	70.9

Table 1 Weights of the different manufactured panels.

# 3. Methods

## 3.1. Roughness analysis of AD cross-section

The first data collected are related to the surface roughness of the AD ring's cross-section. An Alicona microscope is used for the quantitative aspects and a three-dimensional mapping, while a qualitative analysis is previously made with a Nikon Eclipse LV150 with a 5xlens.

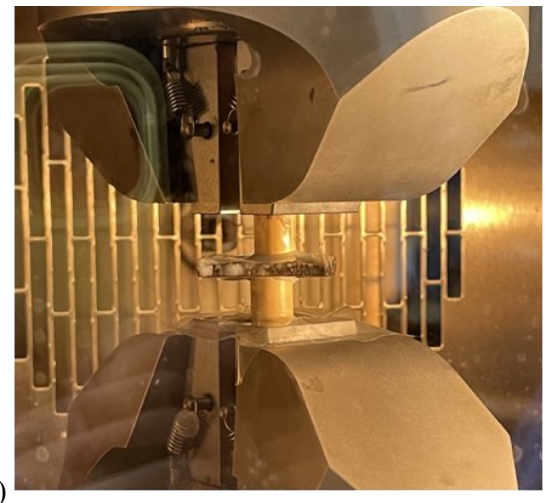
A quantification of the surface roughness is given by Surface Portance, which indicates the percentage of the surface (calculated in  $\mu$ m) which are upper and under the middle plane.

All the specimens used for the pull-off test were tested, in particular three measurements per each sample's CSS were analyzed.

## 3.2. Pull-off tests

Pull-off tests are performed to understand the influence of the surface treatment of AD cross section on the resistance.

Two AD rings are glued to a 3cm x 3cm of flax skin obtained with 25 layers of flax (about 4mm thick), ensuring sufficient thickness to avoid its failure (as shown in Figure 6(a)). The combination of PB170 (5g) and the hardener DM02 (1.8g) is used as foaming glue. The samples are placed into clamps supports of the machine, then the glue is solidified for one hour in the preheated oven at 100°C under a compression load of 50 N (Fig. 6b)). The Pull-off tests were performed at room temperature with Instron Electropulse E 10000 (Fig. 6 (a)) on different samples with different polishing treatments on their cross-section. In particular, the pull-off tests were performed on two non-polished samples, two polished samples with P120 sandpaper, and two polished samples with P400 sandpaper. The pull-off test is performed in displacement control with a velocity of 0.60 mm/min.



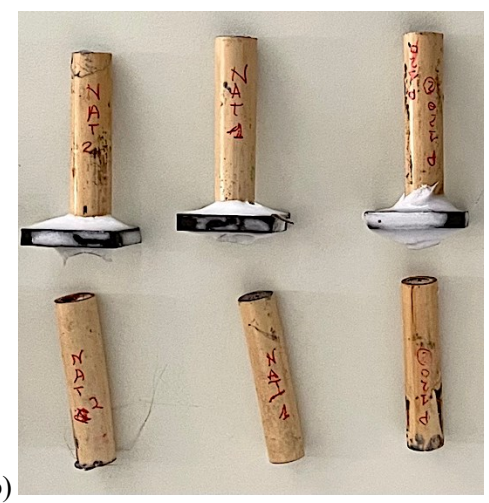


Figure 6 (a) Sample in the oven at 100°C before the pull-off test; (b) Samples after the pull-off test.

# 3.3. Three-points bending test

The three-point bending tests were performed on samples of the whole sandwich of about 300mm x 35mm x 14mm. At least 4 specimens from each manufactured panel were tested. The procedure follows the ASTM C393-00 [24] standard for the three-point bending test for long beam three-point load (Fig. 7). The span length is 220mm and the displacement rate of 6 mm/min. Tests were carried out on a universal testing machine MTS criterion 45 equipped with a 5 kN full-range load sensor. The deflection was measured at mid-span, on the bottom face of the specimen, using a micrometer laser sensor (microepsilon optoNCDT 1420).



Figure 7 Three-point bending test setup.

The test was performed on sandwich samples with a core made with AD rings that had undergone different polishing treatments on the lateral surface.

The core shear stress, the skin bending stress, the flexural strain and stress and the tangent modulus of elasticity are calculated following the Standard Test Methods for Flexural Properties ASTM D790-03 [25].

The core shear stress  $\tau$  is expressed as

$$\tau = \frac{P}{(d+c)\,b}$$

where P is the load, d is the sandwich thickness, c is the core thickness, and b is the sandwich width. The skin bending stress  $\sigma$  is expressed as

$$\sigma = \frac{PL}{2t (d+c) b}$$

where t is the skin thickness, and L is the span length.

The flexural stress  $\sigma_f$  and strain  $\varepsilon_f$  are expressed as

$$\sigma_f = \frac{3 PL}{2 b d^2}$$

$$\varepsilon_f = \frac{6 \, Dd}{L^2}$$

where D is the deflection and L is the span length. The modulus of elasticity in bending  $E_B$  is expressed as

$$E_{\rm B} = \frac{L^3 m}{4 b d^3}$$

where m is the slope of the tangent to the initial curve of the load.

## 3.4. Analytical Model

To study the behaviour of a panel under the three-point bending test, two analytical models were developed: the equivalent panel model, which considers a homogenised material, and the sandwich

model is based on sandwich theory. For both models, a linear elastic behaviour is considered. The sandwich panel theory [26], allows for calculating the equivalent flexural stiffness (EI)<sub>eq</sub> as:

$$(EI)_{eq} = \frac{E_{c2}bc^3}{12} + 2 \cdot \frac{E_{f1}bt^3}{12} + 2 \cdot E_{f1}bt \left(\frac{d}{2}\right)^2$$

where  $E_{f1}$  is the Young modulus of the skins along the longitudinal axis of the panel and  $E_{c2}$  is the Young modulus of the core material along the longitudinal axis of the panel, the meaning of the symbols b, c, d and t reported above are explained in the paragraph 3.3. The sandwich model can be further exploited under the hypotheses  $E_{f1} \gg E_{c2}$  and  $c \gg 2t$ , the rigidity  $(EI)_{eq}$  can be approximated as:

$$(EI)_{eq} = \frac{E_{f1}btc^2}{2}.$$

 $(EI)_{eq} = \frac{E_{f1}btc^2}{2}.$  According to this theory, the skins absorb all the normal stress acting on the panel, while the core absorbs the tangential stress.

The normal stress acting in the skin,  $\sigma_s$  is calculated as [26]:

$$\sigma_S = \frac{M}{b \cdot t \cdot c}$$
;

where M is the bending moment acting on the beam. The deflection at the midpoint of the beam is given by the sum of a bending contribution related to the skins and a shear contribution associated with the core  $\delta = \delta_b + \delta_s$ , where:

$$\delta_b = \frac{P \cdot L^3}{48 \cdot (EI)_{eq}}; \, \delta_S = \frac{P \cdot L}{4 \cdot G_C \cdot A_C}$$

where  $G_c$  is the shear modulus of the core, and  $A_c$  is the shear area, and P is the load. In the equivalent model, based on the equivalent panel theory, the panel is considered made of a single

equivalent homogeneous and isotropic material with the following equivalent Young modulus  $\tilde{E}$ obtained by enforcing the equality with the bending stiffness of the sandwich model  $(EI)_{eq}$  as:

$$\tilde{E} = \frac{(EI)_{eq}}{\tilde{I}}; \tilde{I} = \frac{bd^3}{12}$$

where  $\tilde{I}$  is the inertia moment of the equivalent cross-section of the panel, considered homogeneous.

#### 3.5. Finite Element Model (FEM)

Two finite element models have been developed, one for the case of non-polished panels and one for the case of polished panels P120 by using Abaqus software. Figure 8. shows the 3D model. The skin and the Arundo donax ring walls are modelled as orthotropic materials and considered to maintain a linear elastic behaviour until the failure of the panel.

The core was modelled using rings with constant diameters of 15mm, this size was chosen as it represents the average diameter of rings used in experimental settings. The thickness of the walls ring was set at 1/10 of the diameter, which is 1.5 mm. The arrangement of the rings is regular, meaning they were arranged along three rows covering the entire length of the panel. Half of the panel is modelled using symmetric boundary conditions to represent the three-point bending.

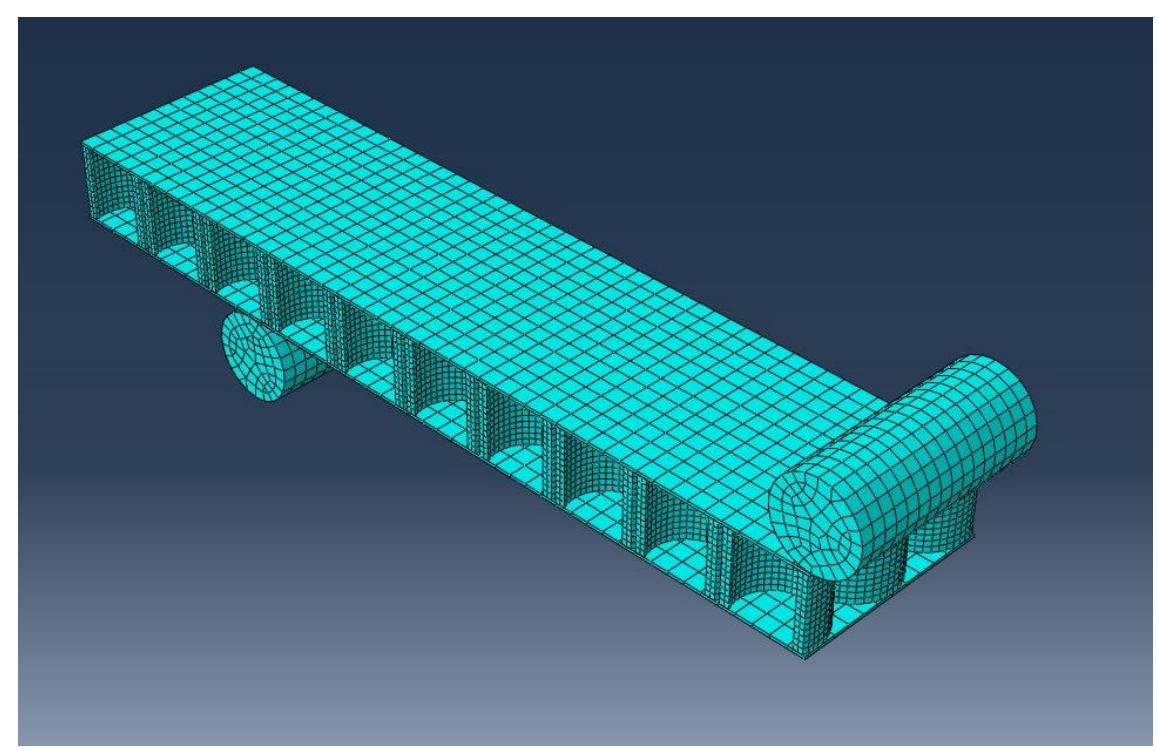


Figure 8 Finite Element Model (FEM) of a sandwich beam under a three-point bending test

The engineering constants of the Arundo donax and the flax-reinforced composite used in the FEM are taken from [11] and [27], respectively, and are reported in Table 2.

Parameter	Definition	Value	
		Arundo donax	Flax composite
$\overline{E_{11} \text{ [GPa]}}$	Longitudinal elastic modulus	13.4	36.0
$E_{22} = E_{33} [\text{GPa}]$	Transverse elastic modulus	1.05	4.20
$v_{11} = v_{22} = v_{33}$	Poisson's ratio in plane 1-2/1-3/2-3	0.57	0.33
$G_{12} = G_{13} = G_{23}$ [GPa]	Shear modulus in plane 1-2/1-3/2-3	2.96	4.29

Table 2 Engineering constants are considered in the FE model for the facial and core materials.

A Poisson's ratio equal for the minor and major ratios was used, as it was referenced in the article by L. Ávila de Oliveira et al. 2020 [28]. The supports of the beam and the load cell are modelled as cylindrical rigid shells, to which boundary conditions are applied through reference points (RP). Constraints have been imposed on the supports, while the load cell is allowed to translate in the direction transverse to the longitudinal direction of the specimen. Cohesive surfaces are used to model the contact between the skins and the Arundo rings of the core. The contacts between the skins and the support and skin/indenter are modelled using hard contact in the normal direction and friction in the tangential direction.

Parameter	Definition
$K_1; K_2; K_3 \text{ [N/mm}^3]$	Penalty stiffness
$t_1; t_2; t_3$ [MPa]	Damage initiation stress
$g_1; g_2; g_3$ [N/mm]	Fracture energy
μ	Viscosity

**Table 3** Cohesive zone parameters were used in the model.

Table 3. shows the cohesive zone parameters: the Damage initiation stress in the normal direction  $t_1$  and the transverse direction  $t_2$  and  $t_3$  expressed in [MPa]; the Fracture energy in the normal direction  $g_1$  and

transversely  $g_2$  and  $g_3$  expressed in [N/mm], and the Penalty stiffness of the cohesive layer in the normal direction  $K_1$  and the transverse direction  $K_2$  and  $K_3$ . These interface properties are dependent on the type of adhesive utilized. The viscosity coefficient  $\mu$  stabilizes the material in a softening regime, it is set equal to 0.0005 as suggested by Demir et al. 2018 [29] after performing a detailed analysis of the influence of the viscosity coefficient on the results.

Flax composite skins and Arundo rings of the core are modelled using an eight-node linear brick 3D element (C3D8R).

The difference between the two models lies in the fact that in the first case, it was assumed that there is no interaction between the resin and the rings inside the core, nor between the rings themselves; hence, each ring behaves as a separate entity. In the case of the polished P120 model, however, it was hypothesized that the same interaction present between the skins and the core also exists between the rings within the core, due to improved grip between the resin foam and the rings. Therefore, the rings function as a unified element.

Another difference between the two models concern the geometric characteristics of the modeled panel, which refer to the averages of the tested samples. In the case of the non-polished panel, the base is 32.9 mm, and the thickness of the skins is 0.6 mm, while for the polished P120 case, these dimensions are 35 mm and 0.5 mm, respectively.

#### 4. Results

## 4.1. Analysis of the cross-section surface

The analysis of the surface roughness of AD ring cross sections non-polished and polished is performed. Fig. 9(a) and (b) show the images taken with Nikon Eclipse LV150 with a 5x lens cross-section before polishing and after polishing with P120 sandpaper and the difference is evident.

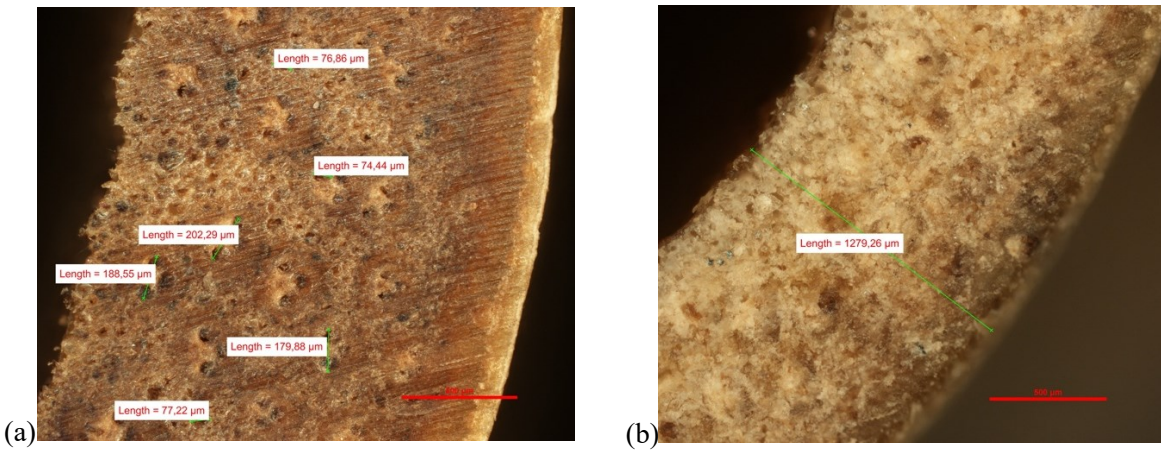
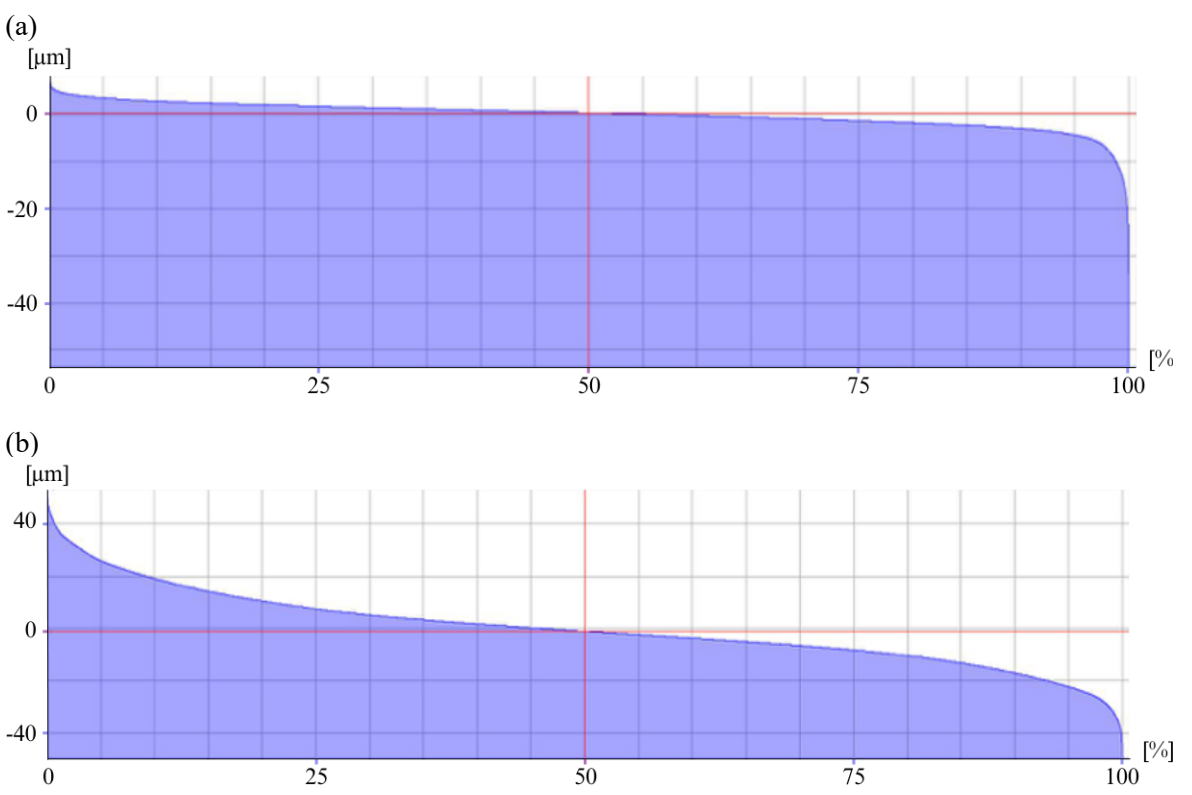


Figure 9 (a). Non-polished cross section's surface; (b) Polished cross section's surface with P120 sandpaper

Fig. 10(a) and (b) report an example of the Surface Portance around a point of non-polished samples and polished samples respectively (the same difference in the graphs is obtained in other points). It is clear that the difference in the topography in polished samples is greater than that in polished ones.



**Figure 10** (a) Depth [ $\mu$ m] vs Surface Portance [%] for polished specimens; (b) Depth [ $\mu$ m] vs Surface Portance [%] for non-polished specimens.

# 4.2. Pull-off tests

Table 4 synthetises the maximum load reached during the pull-off tests. It shows that samples polished with P120 sandpaper on the CSS exhibit higher resistance compared to non-polished samples (the increment goes from 22.83% to 52.88% depending on samples).

Fig. 11 (a) shows the P120 polished sample and Fig. 11 (b) the non-polished sample. The polished P120 samples have a substrate of the flax skin which covers almost the entire surface of the samples, while the non-polished samples have a cohesive failure of the glue substrate only a few flax fibres can be noted on the surface. For this reason, all the Arundo donax rings of the core have been polished with P120 sandpaper on their cross sections.

<b>Cross-section treatment</b>	Maximum load [N]
Non-polished 1_CS	385.2
Non-polished 2 CS	235.2
P120 1_CS	499.1

**Table 4** Pull-off test results comparing the specimens with similar cross section's dimensions.

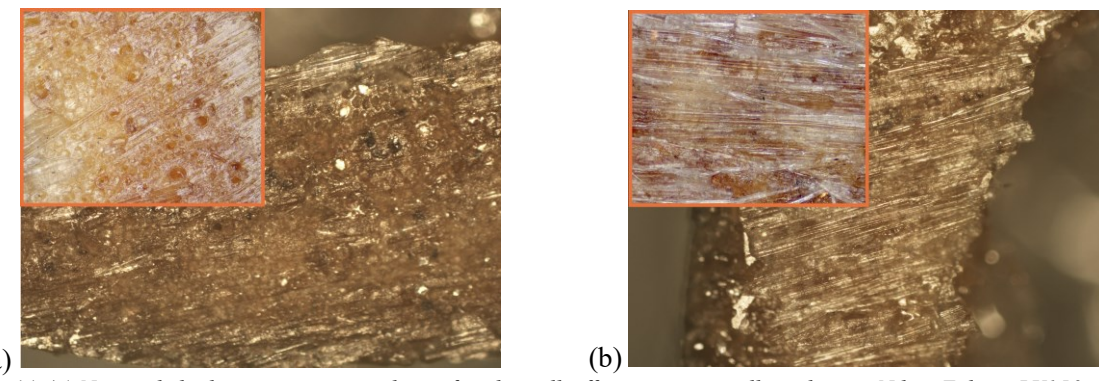


Figure 11 (a) Non-polished cross section analysis after the pull-off test, images collected using Nikon Eclipse LV150 with a 5x lens; (b) P120 polished cross section analysis after the pull-off test, images collected using Nikon Eclipse LV150 with a 5x lens

# 4.3. Three-points bending tests

Fig. 12 shows the load-deflection and Table 5 synthetises deflection, load, core shear stress, skin bending stress, flexural stress, and strain and modulus of elasticity.

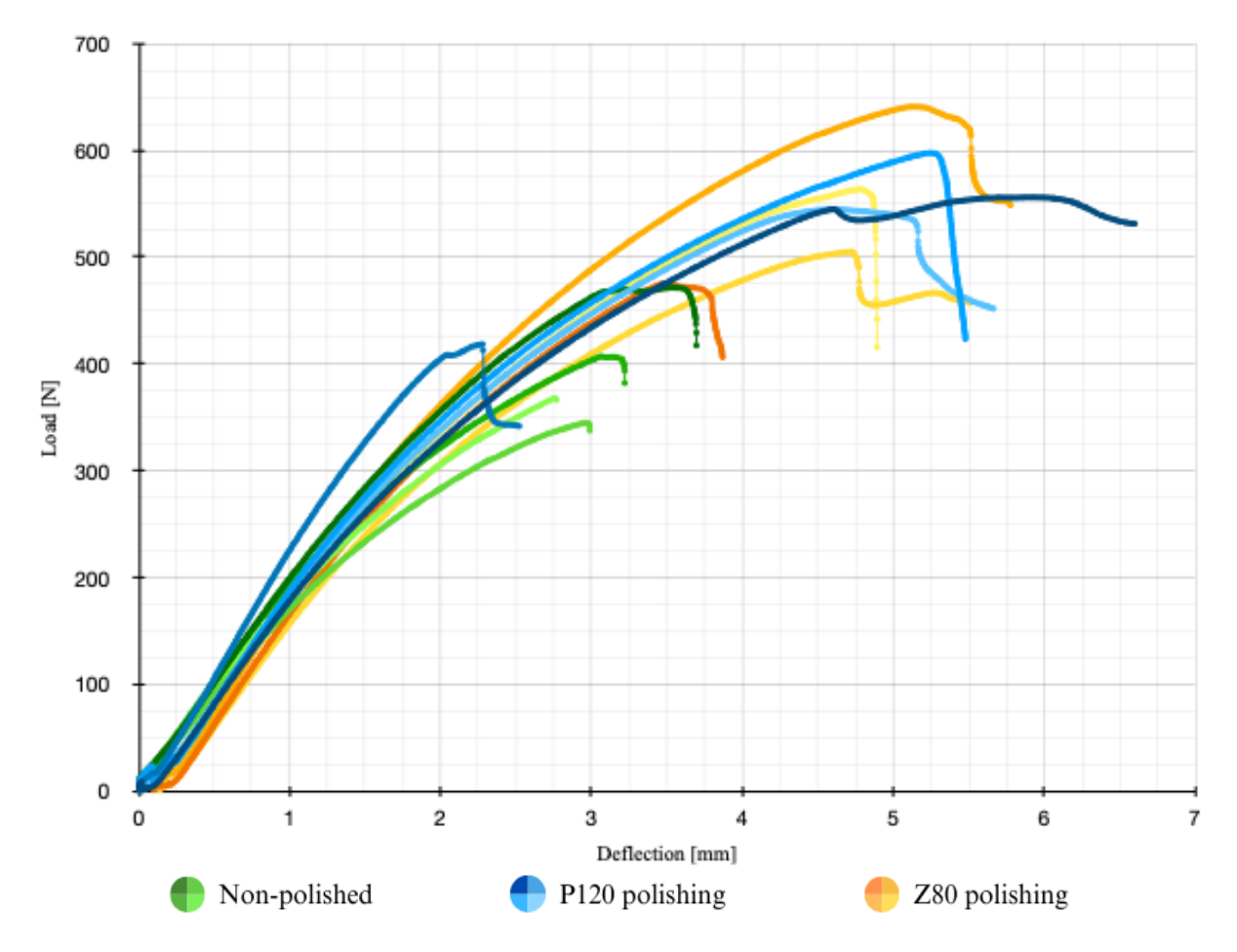


Figure 12 Load-displacement curves.

Specimens	Deflection [mm]	Load [N]	Core shear stress, τ <sub>c</sub> [MPa]	Skin bending stress os [MPa]	Flexural strength σ <sub>f</sub> [MPa]	Elasticity modulus E <sub>B</sub> [GPa]	Flexural Strain ε <sub>f</sub>
Non-polished1_LS	3.44	471.1	0.53	48.43	23.14	4.93	0.61
Non-polished2_LS	3.17	406.4	0.44	40.60	19.28	4.39	0.57
Non-polished3_LS	2.98	344.7	0.38	35.33	16.35	3.86	0.53
Non-polished4_LS	2.73	367.6	0.41	37.34	17.45	4.14	0.49
Mean	3.08	397.5	0.44	40.43	19.06	4.33	0.55
St.dev	0.30	55.3	0.06	5.76	2.98	0.45	0.05
Z80 1_LS	3.20	475.0	0.50	49.66	22.47	4.98	0.56
Z80 2_LS	4.90	640.5	0.66	73.17	30.12	5.50	0.85
Z80 3_LS	4.42	504.8	0.53	58.05	23.83	4.71	0.77
Z80 3_LS	4.58	563.3	0.59	64.95	26.65	5.05	0.79
Mean	4.28	545.9	0.57	61.46	25.77	5.06	0.74
St.dev	0.74	72.9	0.07	10.01	3.38	0.33	0.13
P120 1_LS	5.85	555.8	0.59	64.69	26.40	4.77	1.02
P120 2_LS	2.17	418.2	0.44	48.36	19.97	6.03	0.37
P120 3_LS	5.11	597.4	0.63	68.87	28.28	5.15	0.88
P120 4_LS	4.52	544.6	0.57	63.17	25.99	4.93	0.78
Mean	4.41	529.0	0.56	61.27	25.16	5.22	0.76
St. Dev.	1.59	77.2	0.08	8.94	3.60	0.56	0.28

**Table 5** Three-point bending tests: deflection, load, core shear stress, skin bending stress, flexural stress and strain and modulus of elasticity.

The average maximum load increases from 397.5 N for the non-polished samples to 545.9 N and 529 N for the samples with the rings' lateral surfaces polished with Z80 and P120 sandpapers, respectively. All the mechanical characteristics increase with the polishing treatment of the lateral surface, with an increase from 0.44 MPa to 0.56 and 0.57 MPa for the average values of the core shear stress, from around 40 MPa to 61 MPa for the skin bending stress, from 19 MPa to around 25 MPa for the flexural stress and from 4 GPa to 5.1 and 5.2 GPa for the flexural Young modulus. This increase in shear rigidity and strength in the core of the sample, is a consequence of the better adhesion between the rings and the higher bending stress in skins, since the load shows a better transferring from the core and the skins. The data obtained with the Arundo donax core are higher than those obtained with a similar setup with rings bamboo core in de Oliveira et al. [28], where the average flexural strength reached around 9 MPa and an average flexural modulus around 3.2 GPa. This difference is attributed to the core material, as de Oliveira et al. [28] used rings from a bamboo species (Bambusa tuldoides), arranged in three lines. In this paper the setup does not follow any geometrical pattern, but the paramount objective was to reach the maximum lateral surface's contact area between the core rings. In this case, the adhesion related to the rings' contact and the bond created by the foaming glue used between the skins and the core is improved. This enhancement is also due to the fact that the contact surfaces between the skins and the core were polished with sandpaper, and in Z80 and P120 specimens also the lateral surfaces were polished as well.

The lateral surface polishing treatment setup leads to different failure modes. In the four non-polished samples, as shown in Fig 13(a), the main failure mode is debonding between the skins and the AD rings. The failure starts from the core, on the lateral surfaces of the rings and there is the debonding of the skins from the core. In the specimens with the polished lateral surface a similar behaviour is encountered with a buckling failure in the skin (as can be seen in Figs. 13(b) and (c)). This means that failure is not due to the core.

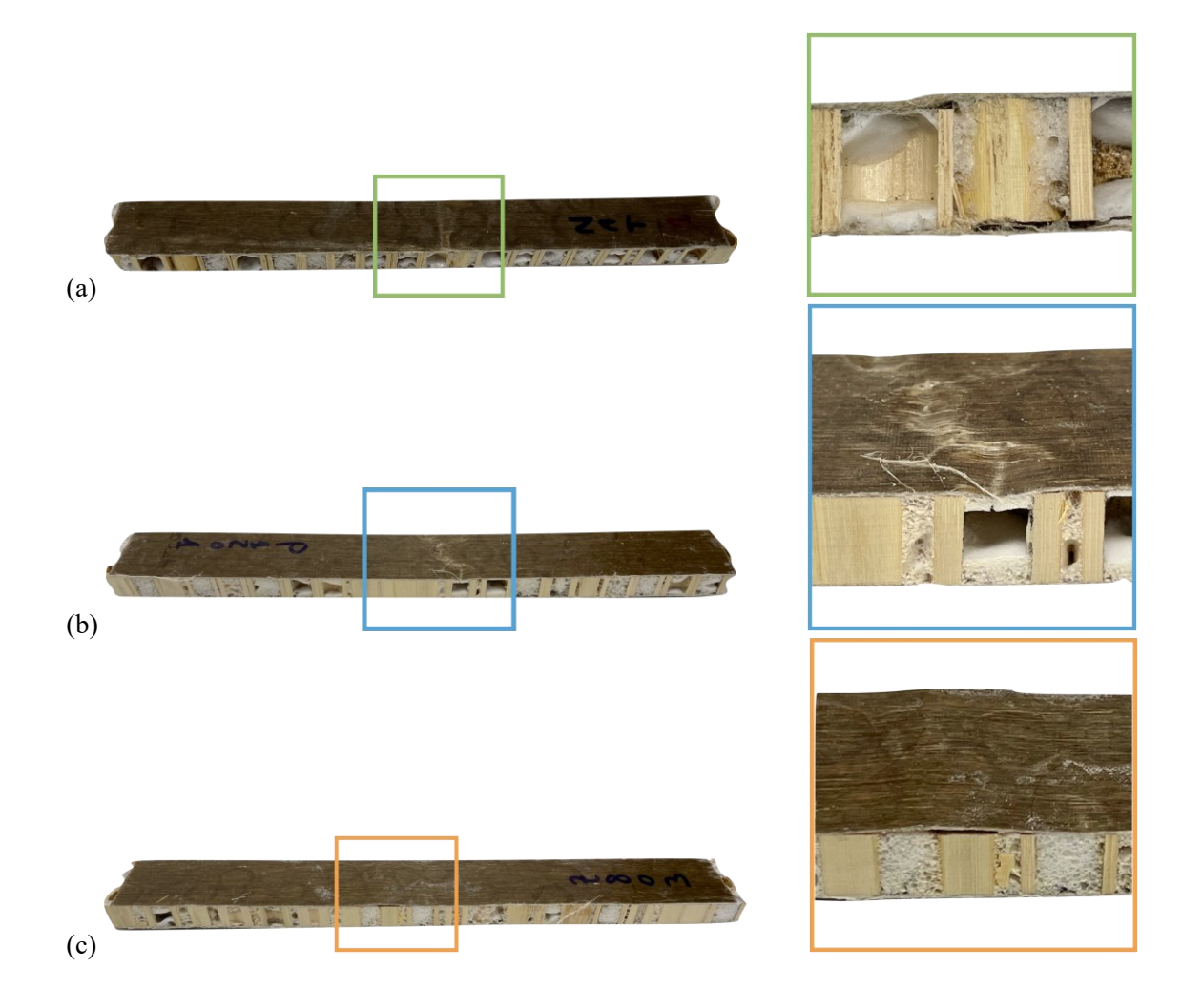


Figure 13 (a) Failure mode for non-polished lateral surface; (b) Failure mode for P120 polished lateral surface; (c) Failure mode for Z80 polished lateral surface.

# 4.4. Results of the bending behaviour of the developed sandwich panels

In the initial phase, the modelling was done for non-polished the samples. The decision was made to start by modelling the non-polished case because, in this instance, the initial hypothesis of the absence of cohesive bonding within the core holds true. In other words, each ring is glued exclusively to the skins and not to other rings within the core or to the foam resin present in the core. Consequently, the maximum tensile stress in the cohesive zone between the rings and the skin will be equal to the tensile stress value obtained from the Pull-off test. The average considered geometric dimensions are reported in Table 6.

Parameter	Definition	Value
$L_{tot} [mm]$	Length	296.5
b [ <i>mm</i> ]	Width	32.9
h [mm]	Panel thickness	14.3
c [mm]	Core thickness	13.1
$D_r[mm]$	Diameter of the ring	15
s [mm]	Wall thickness of the ring	1,5
t [mm]	Skin thickness	0.6
m [g]	Mass	53.6

$\tilde{\rho}$ [g/cm <sup>3</sup> ]	Equivalent Density	0.383
E <sub>f1</sub> [MPa]	Young modulus of the skin	36000
Ec2 [MPa]	Young modulus of the core	13400
$(EI)_{eq}$ [Nmm <sup>2</sup> ]	Flexural stiffness of the sandwich panel	60420448.8
$\tilde{E}$ [MPa]	Young modulus of the equivalent panel	7606

Table 6 Average geometrical and mechanical data for non-polished specimens.

Figure 14 compares load versus displacement curves between the experimental data, the equivalent panel model, and the sandwich theory. The related data are reported in Table 7. The sandwich model replicates the experimental trend in the linear portion of the experimental curve; however, the two trends start to diverge once the nonlinear behaviour of the panel emerges.

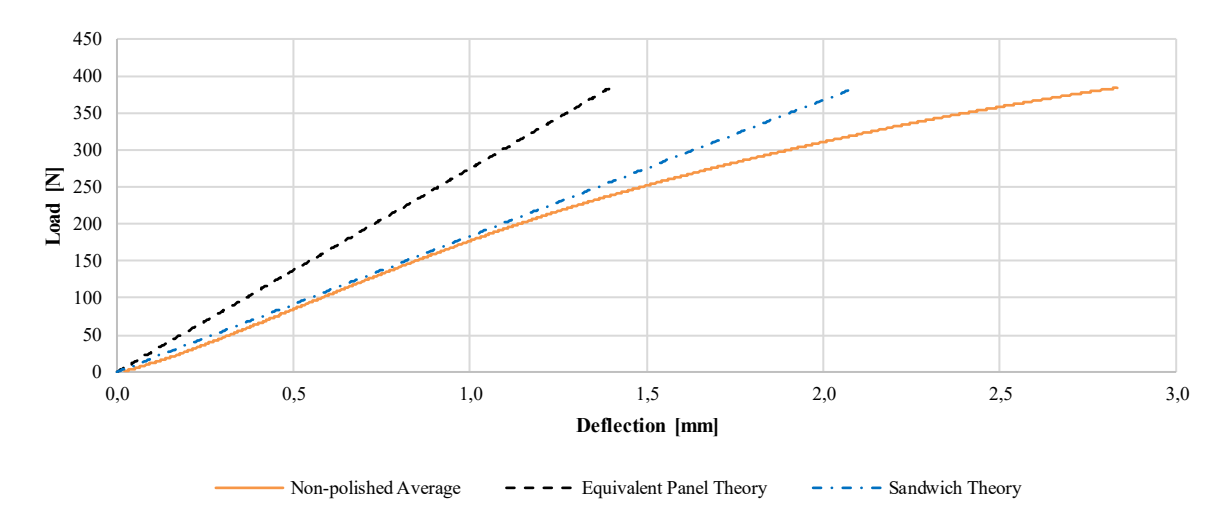


**Figure 14** Comparison of the Load-Displacement curves from the experimental data of Non-polished specimens, Equivalent Plate Theory, and Sandwich Panel Theory.

Parameter	Definition	Value		
		Experiment	Equivalent panel	Sandwich panel theory
δ [mm]	Maximum Deflection	2,83	1,40	2,23
P [N]	Maximum Load	383,9	384,0	384,0
3	Deformation at fracture	0,00502	0,00248	0,00395
$\sigma_s$ [MPa]	Maximum tensile stress of the skin	78,07	/	81,67

Table 7 Output data of the average of the non-polished specimens, equivalent panel model and Sandwich model.

As expected, due to the linear elastic hypothesis and the homogeneous core hypothesis, the analytical models of the sandwich panel are only able to predict the bending rigidity in the linear region of the experimental curve. To better represent the nonlinear behavior of the panel, a FEM model was used. For the non-polished specimens, the parameters of the cohesive zone used in the FE model are reported in Table 8.

Parameter	Definition	Value
$\overline{K_1; K_2; K_3  [\text{N/mm}^3]}$	Penalty stiffness	140
$t_1; t_2; t_3 \text{ [MPa]}$	Damage initiation stress	10,6
$G_1$ ; $G_2$ ; $G_3$ [N/mm]	Fracture energy	2,5
ν	Viscosity	0,0005

**Table 8** Cohesive zone parameters, for the non-polished series.

The damage initiation stress  $t_i$  is derived from the pull-off tests:

$$t_i = \frac{P_{max}}{A}$$

where  $P_{\text{max}}$  is the maximum load applied to the contact area and A is the cross-sectional area. The value of the penalty stiffness K and the fracture energy g were obtained through a tuning process of optimizing the model's output results.

Figure 15. reports the comparison in terms of load versus displacement curves between the Experiment (Average Non-polished) obtained by the three-point bending tests and the Finite Element Model (FEM).

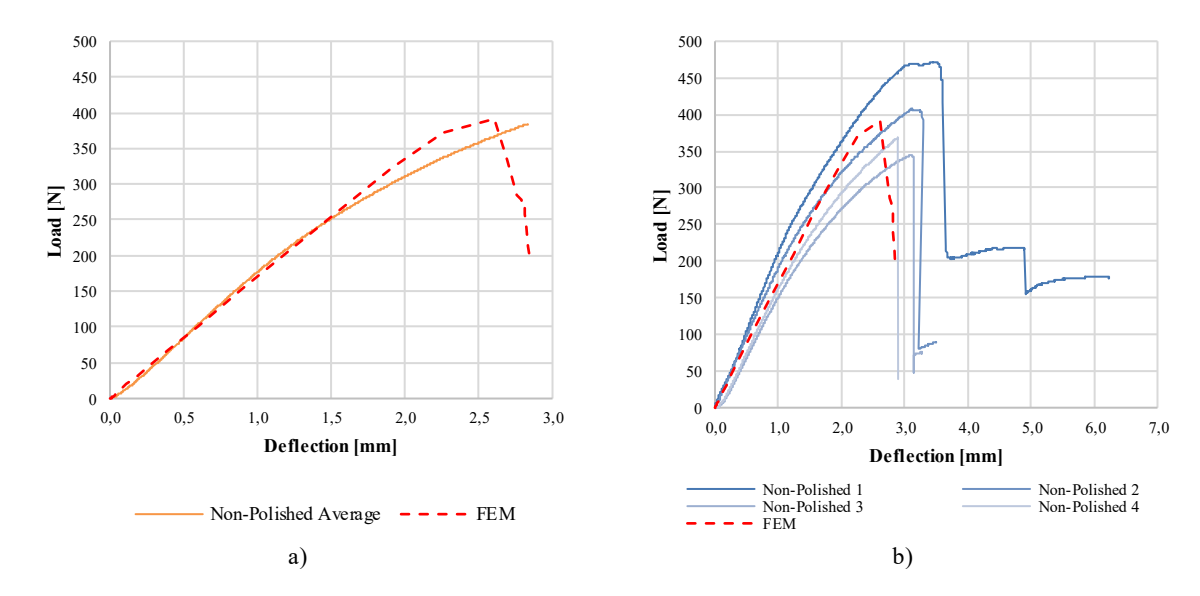


**Figure 15** Comparison between the load-displacement curves: a) of the specimen Average Non-polished and the FE model; b) of all the specimens Non-polished and the FE model.

The trend of the load-displacement curve associated with the FE model optimally simulates the linear part of the graph; however, regarding the nonlinear part, the simulation is less accurate. In the experimental case, there is a greater reduction in stiffness compared to the numerical model. Nevertheless, the deviation between the average experimental curve and the one related to the FEM model falls within the variability of the experimental data for the 4 tested panels, as it is possible to see from Figure 15(b).

Parameter	Definition	Value		
		Non-polished	FEM	
δ [mm]	Deflection at fracture	2,83	2,61	
P [N]	Maximum Load	383,9	391,3	
$\epsilon_{ m f}$	Deformation at fracture	0,00502	0,00462	
$\sigma_{s}$ [MPa]	Maximum tensile stress of the skin	78,07	82,90	

From the data in Table 9, it is evident that the FEM model closely replicates the output of the experimental analysis, particularly the value of the maximum load and the stress in the skins. The failure of the panel, in the case of the FE model, occurs in the connection regions between the skins and the core. The activation of this phenomenon in the model indicates the activation of the failure criteria and degradation law in the cohesive elements of the Finite Element Model (FEM). This is in line with what was obtained experimentally.

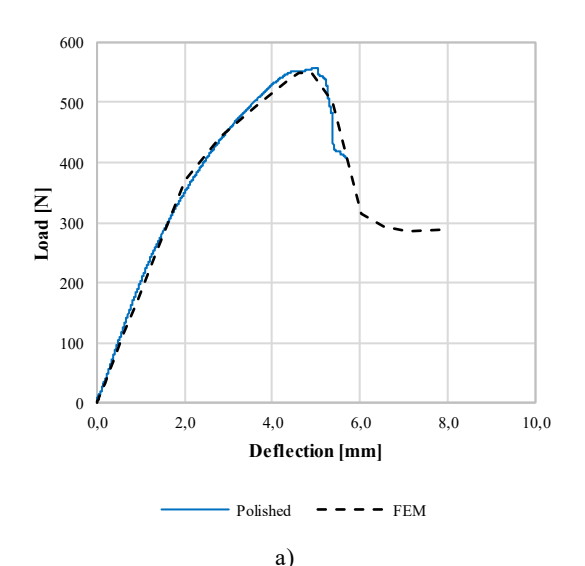
Once the modelling associated with the non-polished series panels was completed, modelling was also carried out for the polished P120 series panels. For these panels, it was decided to keep the same parameters of the cohesive zone obtained for the non-polished case, except for the Damage initiation stress t, which was obtained through a tuning process. The values of the cohesive zone parameters for the P120 case are reported in Table 10. The value of t appears to be significantly greater compared to the Non-polished case.

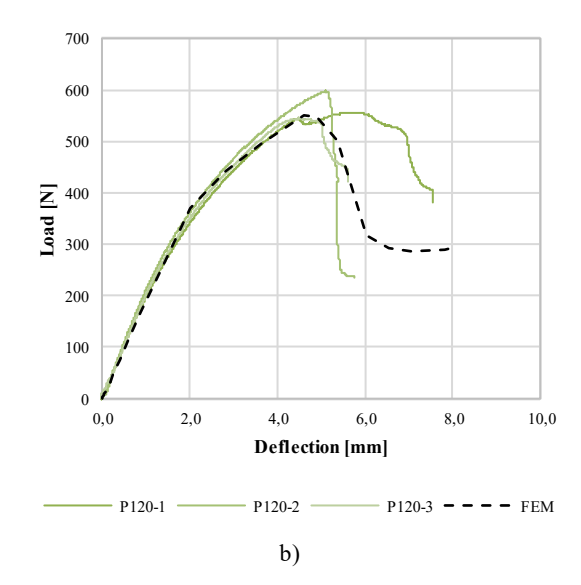
Another difference compared to the previous model is the inclusion of cohesive interaction within the core of the panel between a ring and its adjacent rings, resulting in a cohesive core.

Parameter	Definition	Value
$K_1; K_2; K_3 \text{ [N/mm}^3]$	Penalty stiffness	140
$t_1; t_2; t_3 \text{ [MPa]}$	Damage initiation stress	36
$g_1; g_2; g_3$ [N/mm]	Fracture energy	2,5
μ	Viscosity	0,0005

**Table 10** Cohesive zone parameters, for the polished series.

Figure 16 reports the comparison in terms of load versus displacement curves between the Experiment (Average polished) obtained by the three-point bending tests and the Finite Element Model (FEM).





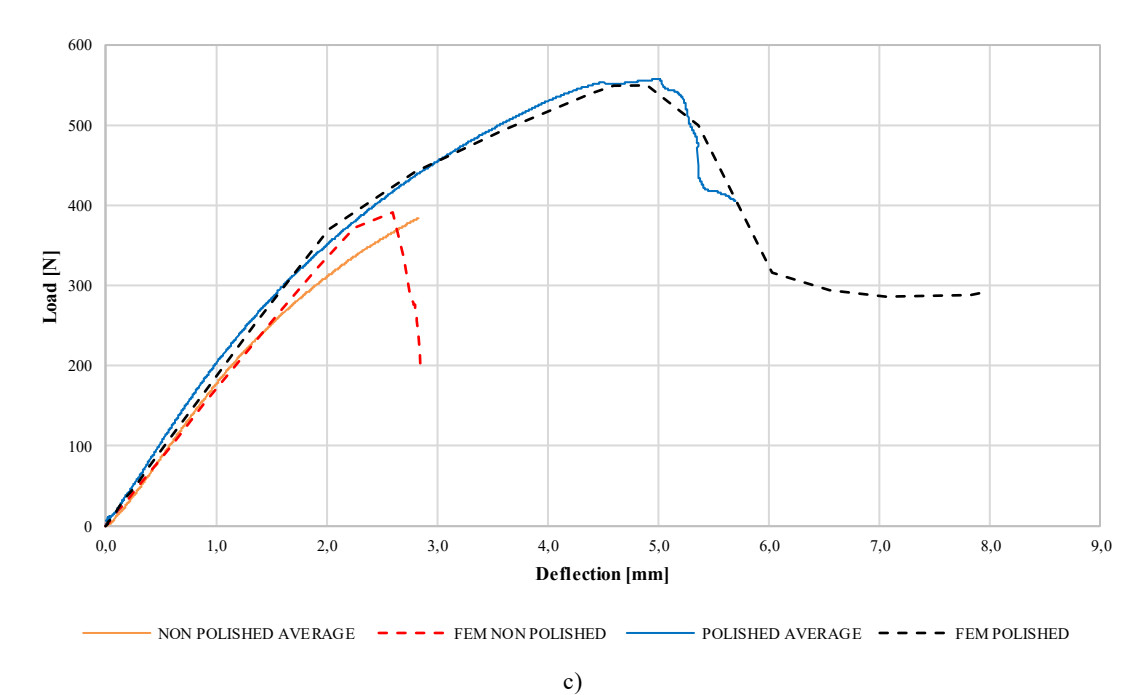


Figure 16 Comparison between the load-displacement curve: a) of the specimen Average P120 and the FE mode; b) of all the specimens P120 and the FE model; c) Comparison between the Average and FE models for the Non-polished and Polished specimens.

From Figure 16(a) and 16(b), it is possible to observe that the model reproduces the behavior of the panel under a three-point bending test, both in the linear, non-linear and failure parts. The FEM model for specimen P120 presents a very low discrepancy from the experimental values, as can be observed from Table 11, even regarding the stress values in the skins. In Figure 16 (c), a comparison is shown between the average output data from the three-point bending test for the experimental part and the outputs, represented with dashed lines, related to the models for the non-polished panel case and the polished P120 panel case.

Parameter	Definition	Value	
		P120	FEM
δ [mm]	Deflection at fracture	5,01	4,60
P [N]	Maximum Load	557,34	549,26
$\epsilon_{ m f}$	Deformation at fracture	0,0087	0,00815
$\sigma_s$ [MPa]	Maximum tensile stress of the skin\	128,91	129,25

Table 11 Comparison output data between the specimen average P120 and the FE model.

From Figure 16(c), it is possible to compare the load-displacement curves of the averages of the Non-polished and Polished specimens and their respective FEM models. In the experimental part, following the roughening of the lateral surfaces of the Arundo donax rings, the panel subjected to a three-point bending test shows an increase in ultimate tensile strength as well as an increase in stiffness.

The FEM model associated with the non-polished panels accurately reproduces the linear behaviour and reasonably captures the non-linear behaviour of the material, which is an excellent outcome considering the various simplifying assumptions adopted in the model development. Furthermore, the model effectively represents the material's non-linearity and failure, confirming the earlier hypothesis of the complete absence of adhesion between the resin foam and the rings within the core.

In the FEM model, the transition from the Non-polished to the Polished model showed a significant increase in the ultimate strength of the panel, mirroring the experimental case very closely.

The model, thanks to the presence of the cohesive bond within the core, accurately represents the stiffness of the panel.

The increase in material stiffness from non-polished to polished is due to the proper adhesion between the foam resin and the Arundo rings constituting the core, which occurs once the lateral surface of the rings undergoes the polishing treatment. This adhesion does not occur in the natural state because of the particularly smooth and glassy surface of the material. The adhesion between the foam and the lateral surfaces of the rings not only increases the panel's stiffness, due to the core acting as a single unit but also causes a change in the internal geometry of the core. This change is because the foam resin is simultaneously connected to one of the two skins and the rings inside the core, transmitting the stresses from the skin to the rings, which then redistributes them to the second skin. This results in an increase in the contact surface between the skin and the core, which is what causes the increase in the material's bending resistance.

## 5. Conclusions

A new panel with a core made of Arundo donax rings and skins made of flax fibers and epoxy resin is proposed.

The panel was produced and tested through a three-point bending test. The panel showed good bending properties, what makes it suitable for replacing non-structural and structural panels in the construction industry, such as chipboard panels, whose minimum strength requirements for both cases are specified in the EN 312 standard. [29]

Results show that the polishing treatments on the lateral and the cross-section surfaces of the Arundo donax rings influence the mechanical properties of the panel.

In particular, the mechanical characteristics increase with the polishing treatment of the basal and lateral surfaces. Core shear stress, flexural stress, and modulus increase by approximately 30% on average when the facing bending stress increase reaches 52%.

The finite element model accurately predicts load-displacement curves for both types of panel series, non-polished and polished P120. The models can accurately predict both the linear and non-linear behavior of the material, as well as the failure phase.

Initially developed for the non-polished series, by adding the hypothesis of a cohesive interaction between the rings constituting the core of the panel, and assuming that this interaction is the same as the one present between the skins and the core, the model performed well with the P120 polished series, by adjusting only one model parameter: the Damage initiation stress t, which was expectedly higher compared to the non-polished case. The skins and rings were modelled as homogeneous orthotropic solids, utilizing orthotropic properties to match the structure's stiffness effectively.

Through the non-polished model, it was possible to confirm the hypothesis of a complete lack of connection between the foam resin and the lateral surfaces of the rings, meaning that each ring functions as a separate element within the core.

The FEM P120 model allowed for the confirmation that following the polishing treatment of the lateral surfaces of the rings, there is proper adhesion between the resin and the rings. This increases the stiffness of the panel and causes a modification in the internal geometry of the core, resulting in an increased contact surface between the core and the skin. This is responsible for the increased bending resistance of this type of panel compared to the untreated case.

The implementation of cohesive interaction within the core, between the rings that constitute it, was crucial for the correct realization of the model. Without this interaction, the material would be much less rigid than it is.

It was possible to create a model that accurately represents the mechanical behavior of the material, both in the absence of surface treatment and when surface treatment is applied. This was achieved while keeping the model simple and easily reproducible, which was one of the intended objectives.

# Credit authorship contribution statement

**Letizia Crociati:** Conceptualization, Data curation, Formal analysis, Investigation, Methodology, Validation, Visualization, Writing original draft. **Giovanni Donini:** Conceptualization, Data curation, Formal analysis, Investigation, Methodology, Simulation, Validation, Visualization, Writing original draft. **Thomas Jeannin:** Investigation, Methodology, Supervision. **Luisa Molari:** Conceptualization, Investigation, Methodology, Writing — review & editing, Supervision. **Vincent Placet:** Conceptualization, Investigation, Methodology, Writing — review & editing, Supervision.

## Data availability

The data presented in this study are included in the article or data will be made available on request.

#### **Conflict of interest**

The authors declare that they have no known competing financial interests or personal relationships that could have appeared to influence the work reported in this paper.

#### Acknowledgment

The author Letizia Crociati wishes to acknowledge her research's support by the University of Bologna and funded by the European Union - NextGenerationEU with funds made available by the Italian Ministry of University and Research under National Recovery and Resilience Plan (NRRP) Mission 4, Component 2, Investment 3.3 (M.D. 117/2023) and by Sadepan Chimica Srl.

# Glossary

$\tau_{ m c}$					
te.	Core shear stress [MPa]				
P	Load [N]				
b	Sandwich width [mm]				
c	Core thickness [mm]				
d	Sandwich thickness [mm]				
$\sigma_{ m s}$	Skin bending stress [MPa]				
L	Span length [mm]				
t	Skin thickness [mm]				
$\sigma_{ m f}$	Flexural stress of the panel [MPa]				
$\epsilon_f$	Flexural strain of the panel [MPa]				
D	Deflection [mm]				
E <sub>B</sub>	Modulus of elasticity in bending [GPa]				
(EI) <sub>eq</sub>	Flexural stiffness of the panel [GPa]				
$E_{c2}$	Young modulus of the core material along the				
	longitudinal axis of the panel [GPa]				
$E_{f1}$	Young modulus of the skins along the				
,-	longitudinal axis of the panel [GPa]				
δ	Deflection at the midpoint of the beam [mm]				
$\delta_b$	Bending contribution of the deflection [mm]				
$\delta_{s}$	Shear contribution of the deflection [mm]				
$G_c$	Shear modulus of the core [GPa]				
$egin{array}{c} \delta_s \ G_c \ A_c \  ilde{\mathcal{E}} \end{array}$	Shear area [mm <sup>2</sup> ]				
$\mid \widetilde{E} \mid$	Equivalent Young modulus [MPa]				
Ĩ	Inertia moment of the equivalent cross-section				
	[mm <sup>3</sup> ]				
$E_{11}$	Longitudinal elastic modulus [GPa]				
$E_{22}^{11}; E_{33}$	Transverse elastic modulus [GPa]				
$v_{11}; v_{22}; v_{33}$	Poisson's ratio in plane 1-2/1-3/2-3				
$G_{12}; G_{13}; G_{23}$	Shear modulus in plane 1-2/1-3/2-3 [GPa]				

$K_1; K_2; K_3$	Penalty stiffness [N/mm <sup>3</sup> ]
$t_1; t_2; t_3$	Damage initiation stress [MPa]
μ	Viscosity
$g_1; g_2; g_3$	Fracture energy [N/mm]
$L_{tot}$	Length of the panel [mm]
$D_r$	Diameter of the ring [mm]
s	Wall thickness of the ring [mm]
m	Mass [g]
$ \tilde{ ho} $	Equivalent Density $[kg/m^3]$
A	Cross-sectional area [mm <sup>2</sup> ]

# References

- [1] J. Lange, A. Von Der Heyden, S. Grimm Böger, J. Gesellschaft, Sandwich panels in buildings: Core, structure and design, 2019. https://www.researchgate.net/publication/335993008.
- [2] B. Vijaya Ramnath, K. Alagarraja, C. Elanchezhian, Review on Sandwich Composite and their Applications, Mater Today Proc 16 (2019) 859–864. https://doi.org/10.1016/J.MATPR.2019.05.169.
- [3] A. Joseph, Liquid water lake under ice in Mars's southern hemisphere—Possibility of subsurface biosphere and life, Water Worlds in the Solar System (2023) 453–522. https://doi.org/10.1016/B978-0-323-95717-5.00019-0.
- [4] L.B.L. Gato, S.L.M. Ribeiro Filho, T.H. Panzera, M.L.P. Tonatto, A.L. Christoforo, F. Scarpa, Sandwich Structures Made of Discarded Bottle Caps Core and Hybrid Glass Fibre Composite Skins, Applied Composite Materials 28 (2021) 1427–1449. https://doi.org/10.1007/s10443-021-09922-x.
- [5] P.R. Oliveira, M. May, S. Kilchert, L. Ávila de Oliveira, T.H. Panzera, V. Placet, F. Scarpa, S. Hiermaier, Eco-friendly panels made of autoclaved flax composites and upcycled bottle caps core: experimental and numerical analysis, Composites Part C: Open Access 4 (2021). https://doi.org/10.1016/j.jcomc.2021.100114.
- [6] S. Antony, A. Cherouat, G. Montay, Fabrication and Characterization of Hemp Fibre Based 3D Printed Honeycomb Sandwich Structure by FDM Process, Applied Composite Materials 27 (2020) 935–953. https://doi.org/10.1007/s10443-020-09837-z.
- [7] F. Napolitano, J.C. Santos, R.J. da Silva, G.G. Braga, R.T.S. Freire, T.H. Panzera, Sandwich panels made of aluminium skins and gapped-bamboo ring core, Journal of the Brazilian Society of Mechanical Sciences and Engineering 45 (2023) 250. https://doi.org/10.1007/s40430-023-04140-x.
- [8] S. Darzi, H. Karampour, H. Bailleres, B.P. Gilbert, D. Fernando, Load bearing sandwich timber walls with plywood faces and bamboo core, Structures 27 (2020) 2437–2450. https://doi.org/10.1016/j.istruc.2020.08.020.
- [9] Y. Fu, P. Sadeghian, Bio-based sandwich beams made of paper honeycomb cores and flax FRP facings: Flexural and shear characteristics, Structures 54 (2023) 446–460. https://doi.org/10.1016/j.istruc.2023.05.064.
- [10] L. Avila de Oliveira, G. Luiza Corat Coura, M. Luiz Passaia Tonatto, T. Hallak Panzera, V. Placet, F. Scarpa, L. Ávila de Oliveira, G. Luiza Cota Coura, M. Luiz PassaiaTonatto, T. Hallak Panzera, A novel sandwich panel made of prepreg flax skins and bamboo core, 2020. https://hal.archives-ouvertes.fr/hal-02993941.
- [11] L. Molari, F.S. Coppolino, J.J. García, Arundo donax: A widespread plant with great potential as sustainable structural material, Constr Build Mater 268 (2021) 121143. https://doi.org/10.1016/J.CONBUILDMAT.2020.121143.
- [12] E.A. Nurdiah, The Potential of Bamboo as Building Material in Organic Shaped Buildings, Procedia Soc Behav Sci 216 (2016) 30–38. https://doi.org/10.1016/j.sbspro.2015.12.004.

- [13] R. Caponetto, M. Cuomo, M. Detommaso, G. Giuffrida, A. Lo Presti, F. Nocera, Performance Assessment of Giant Reed-Based Building Components, Sustainability 15 (2023) 2114. https://doi.org/10.3390/su15032114.
- [14] J. Rojas-Sandoval, P. Acevedo-Rodríguez, Arundo donax (giant reed), CABI Compendium (2014).
- [15] T. García-Ortuño, J. Andréu-Rodríguez, M.T. Ferrández-García, M. Ferrández-Villena, C.E. Ferrández-García, Evaluation of the physical and mechanical properties of particleboard made from giant reed (Arundo donax L.), Bioresources 6 (2010) 477–486. https://doi.org/10.15376/biores.6.1.477-486.
- [16] E. Cintura, P. Faria, L. Molari, L. Barbaresi, D. D'Orazio, L. Nunes, Characterization of an Arundo donax-based composite: A solution to improve indoor comfort, Ind Crops Prod 208 (2024). https://doi.org/10.1016/j.indcrop.2023.117756.
- [17] D.B. Dittenber, H.V.S. GangaRao, Critical review of recent publications on use of natural composites in infrastructure, Compos Part A Appl Sci Manuf 43 (2012) 1419–1429. https://doi.org/10.1016/j.compositesa.2011.11.019.
- [18] A. Stamboulis, C.A. Baillie, T. Peijs, Effects of environmental conditions on mechanical and physical properties of flax fibers, Compos Part A Appl Sci Manuf 32 (2001) 1105–1115. https://doi.org/10.1016/S1359-835X(01)00032-X.
- [19] S.H. Aziz, M.P. Ansell, The effect of alkalization and fibre alignment on the mechanical and thermal properties of kenaf and hemp bast fibre composites: Part 1 polyester resin matrix, Compos Sci Technol 64 (2004) 1219–1230. https://doi.org/10.1016/j.compscitech.2003.10.001.
- [20] L. Yan, N. Chouw, K. Jayaraman, Flax fibre and its composites A review, Compos B Eng 56 (2014) 296–317. https://doi.org/10.1016/J.COMPOSITESB.2013.08.014.
- [21] V. Fiore, L. Calabrese, G. Di Bella, T. Scalici, G. Galtieri, A. Valenza, E. Proverbio, Effects of aging in salt spray conditions on flax and flax/basalt reinforced composites: Wettability and dynamic mechanical properties, Compos B Eng 93 (2016) 35–42. https://doi.org/10.1016/J.COMPOSITESB.2016.02.057.
- [22] I. Pillin, A. Kervoelen, A. Bourmaud, J. Goimard, N. Montrelay, C. Baley, Could oleaginous flax fibers be used as reinforcement for polymers?, Ind Crops Prod 34 (2011) 1556–1563. https://doi.org/10.1016/j.indcrop.2011.05.016.
- [23] T. Cadu, M. Berges, O. Sicot, V. Person, B. Piezel, L. Van Schoors, V. Placet, S. Corn, R. Léger, L. Divet, P. Ienny, S. Fontaine, What are the key parameters to produce a high-grade bio-based composite? Application to flax/epoxy UD laminates produced by thermocompression, Compos B Eng 150 (2018) 36–46. https://doi.org/10.1016/J.COMPOSITESB.2018.04.059.
- [24] ASTM, C393-00 Standard Test Method for Flexural Properties of Sandwich Constructions, 2000th ed., 2017.
- [25] Standard Test Methods for Flexural Properties of Unreinforced and Reinforced Plastics and Electrical Insulating Materials 1, n.d.
- [26] H.G. Allen, Analysis and Design of Structural Sandwich Panels, 1st Edition, 1969.
- [27] B. Sala, X. Gabrion, F. Trivaudey, V. Guicheret-Retel, V. Placet, Influence of the stress level and hygrothermal conditions on the creep/recovery behaviour of high-grade flax and hemp fibre reinforced GreenPoxy matrix composites, Compos Part A Appl Sci Manuf 141 (2021) 106204. https://doi.org/10.1016/J.COMPOSITESA.2020.106204.
- [28] L. Ávila de Oliveira, G.L.C. Coura, M.L. PassaiaTonatto, T.H. Panzera, V. Placet, F. Scarpa, A novel sandwich panel made of prepreg flax skins and bamboo core, Composites Part C: Open Access 3 (2020). https://doi.org/10.1016/j.jcomc.2020.100048.
- [29] A. Demir, H. Ozturk, K. Edip, M. Stojmanovska, A. Bogdanovic, Effect of viscosity parameter on the numerical simulation of reinforced concrete deep beam behavior, 2018. www.tojsat.net.

**Sandwich Panel Samples Measurements** 

	Lenght [mm]	Width [mm]	Thickness [mm]	Core thickness [mm]	Skins thickness [mm]	Mass [g]	Equivalent Density [g/cm <sup>3</sup> ]
Non-polished 1	303	32.6	14.3	13.1	1.2	55.5	0.393
Non-polished 2	293	33.3	14.4	13.2	1.2	52.1	0.371
Non-polished 3	295	32.7	14.3	13.1	1.2	53.3	0.386
Non-polished 4	295	33.0	14.3	13.1	1.2	53.4	0.384
Non-polished mean	296.5	32.9	14.325	13.125	1.2	53.575	0.383
Z80 1	300	35.3	14	12.9	1.1	59.8	0.403
Z80 2	300	35.4	14	13	1	59.3	0.399
Z80 3	300	35.3	14	13	1	58.1	0.392
Z80 4	300	35.2	14	13	1	59	0.399
Z80 mean	300	35.3	14	12.975	1.025	59.05	0.398
P120 1	300	35	14	13	1	55.4	0.377
P120 2	300	35.3	13.95	12.95	1	56.3	0.381
P120 3	300	35.4	13.95	12.95	1	58.1	0.392
P120 4	300	35.2	13.94	12.94	1	55.5	0.377
P120 mean	300	35.225	13.96	12.96	1	56.325	0.382

Table A1 Dimensions of the different sandwich panels specimens used for three-points bending test.